ACS APPLIED MATERIALS & INTERFACES

Research Article

www.acsami.org

Optimized Grafting Density of End-Functionalized Polymers to Polar Dielectric Surfaces for Solution-Processed Organic Field-Effect Transistors

Seulyi Lee, Mi Jang, and Hoichang Yang*

Department of Applied Organic Materials Engineering, Inha University, Incheon 402-751, Republic of Korea

Supporting Information

ABSTRACT: Polystyrene (PS) grafted to silicon oxide (SiO_2, referred to as *g*PS-SiO_2) bilayers generated via a polymer grafting method were used as organic-oxide hybrid gate dielectrics to fabricate solution-processed triethylsilylethynyl anthradithiophene (TES-ADT) organic field-effect transistors (OFETs). The dielectric surface properties were significantly altered by the areal grafting densities of different molecular weight (M_w) PS chains with end-functionalized dimethylchlorosilane attached to the SiO_2 surfaces. Lesser grafting densities of longer PS chains increased the surface roughness of the treated SiO_2 surfaces from 0.2 to 1.5 nm, as well as the water contact angles from 94° to 88°. Below a critical M_w of end-functionalized PS, the *g*PS chains on the SiO_2 surfaces appeared to form a brush-like conformation with an areal density value greater than 0.1 chains nm^{-2}, but other high-M_w *g*PS chains formed pancake structures in which the polymeric layers were easily incorporated with solution-processed TES-ADT as a solute. These findings indicate that low-density *g*PS layers interfered with the self-assembly of TES-ADT in cast films, causing great decreases in crystal grain size and π-conjugated orientation. The presence of compact *g*PS chains on the SiO_2 surface could yield high electrical performance of TES-ADT OFETs with a field-effect mobility of 2.1 $cm^2\ V^{-1}\ s^{-1}$, threshold voltage of −2.0 V, and on/off current ratio of greater than 10^7 when compared to those developed using less-concentrated *g*PS-SiO_2 surfaces.

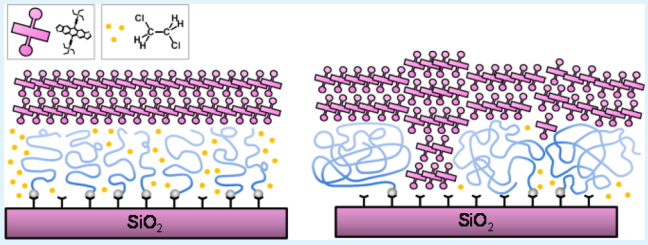

KEYWORDS: *polymer grafting, polymer brush, solution-processed semiconductor, organic field-effect transistor*

1. INTRODUCTION

Organic field-effect transistors (OFETs) have received considerable attention in the past decade due to their potential applications in integrated circuits such as radio frequency identification (RFID) tags, smart cards, and organic active matrix displays.[1,2] The field-effect mobility (μ_{FET}) of OFETs is clearly comparable to that of amorphous silicon-based devices.[3] The μ_{FET} values have been significantly enhanced from less than 10^{-3} $cm^2\ V^{-1}\ s^{-1}$ to more than 10 $cm^2\ V^{-1}\ s^{-1}$, exceeding those of amorphous silicon FETs (μ_{FET} = 0.5−1.0 $cm^2\ V^{-1}\ s^{-1}$).[4−6] These improvements are primarily related to the drastic enhancement of intra- and intermolecular conjugation length of organic semiconductors via synthetic approaches and optimization of the interface engineering between organic semiconductors and dielectrics.[7−9] It is well-known that, in most OFETs, charge-carrier transport is vertically confined within the ultrathin semiconducting layers (<5 nm) near the gate dielectrics, and the surface characteristics of dielectrics are major factors that determine the interfacial trap sites that originate from polar dielectric surface moieties, less-conjugated structures of semiconducting crystallites, and grain boundaries, etc.[10,11]

To minimize the interfacial charge traps, organic self-assembled monolayers (SAMs) or polymeric thin films are introduced into various gate dielectrics, where they provide organo-compatible surfaces to yield less charge-trapping sites.[12−17] End-functionalized polymers have been extensively used as surface modifiers in surface-/interface-related nanoscience and nanotechnology.[18−22] For example, Yang et al. drastically enhanced the organo-compatibility of hydroxyl (−OH)-rich oxide or polymer dielectrics, in which dimethylchlorosilane-end polystyrene PS−$Si(CH_3)_2Cl$ chains were efficiently reacted with the −OH moiety on the surfaces.[22] Because chemical coupling strongly anchored the polymers to the surfaces and unreacted chains were easily rinsed out from the surfaces by solvent cleaning, the grafted polymer (*g*POLY) layers showed excellent solvent resistance without any dewetting or delaminating, even under direct solvent contact.

Because of the bulky characteristics of the polymers, however, many −OH groups on the surface still remained without any chemical coupling. Additionally, when the second polymer- or small molecule-dissolved solutions were subsequently introduced to the *g*POLY layers on substrates, good solvents tended to drastically change the conformation of *g*POLY chains.[23] The surface wettability and interaction then continuously fluctuated during solvent evaporation and were

Received: September 4, 2014
Accepted: October 24, 2014
Published: October 24, 2014

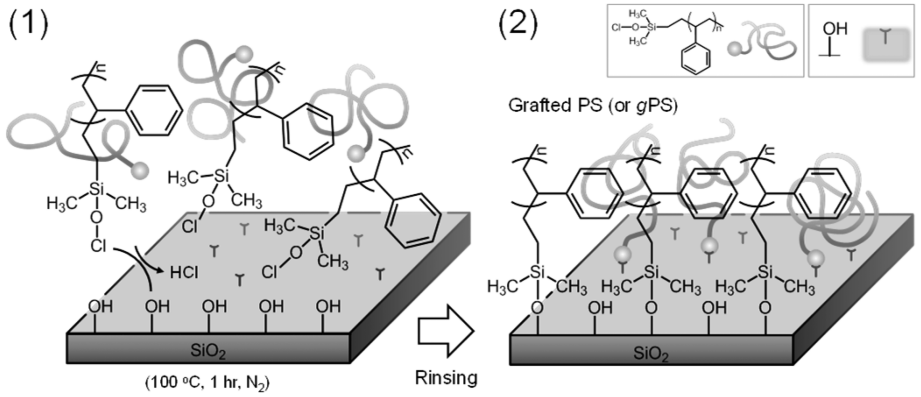

Figure 1. Schemes for PS grafting to the UVO_3-treated SiO_2 surface with popular hydroxyl moieties, via (1) thermal annealing of PS−$Si(CH_3)_2Cl$ film onto the SiO_2 surface at 100 °C for 1 h and (2) solvent-rinsing of the ungrafted polymers.

influenced by the structural order of the polymers attached to the surfaces, which formed "brush" and "pancake" (also referred to as "mushroom")-like structures based on areal graft density (σ), depending on the hydrodynamic size (relative to the radius of gyration, $\langle R_g^2 \rangle^{1/2}$) of the end-functionalized polymers.[24−26] Polymer brushes, in which a densely packed layer of polymer molecules is attached by one end to the surface while the rest of the chain contour is not adsorbed and instead extends out into solution, have become a paradigm for modification of surfaces by attached polymers. In contrast, polymer chains do not overlap with each other at the substrate surface, resulting in the formation of a pancake conformation similar to free polymer chains with a random-coil conformation in solutions of a good solvent.

Concentrated polymer brushes have a unique size-exclusion property against solute molecules in solutions when compared to less-concentrated grafted polymers.[27] When the distance between *g*POLY chains is greater than the size of solute molecules, the solute molecules may be absorbed into *g*POLY, and/or direct adsorption of the solute molecules onto the substrate surface may occur. As a result, the self-assembly of π-conjugated organic semiconductors on the solvent-swollen *g*POLY surfaces during solution film casting will be affected by the grafting density and hydrodynamic conformation of the *g*POLY. Therefore, optimization of polymer grafting to the dielectric surfaces is necessary to achieve high-performance solution-processed OFETs.

In this study, triethylsilylethynyl anthradithiophene (TES-ADT) thin films were fabricated on surface-modified 300 nm-thick SiO_2 dielectrics grafted with different M_w PS−$Si(CH_3)_2Cl$ series. The surface properties of the *g*PS-SiO_2 dielectrics changed considerably, with higher M_w PS−$Si(CH_3)_2Cl$ yielding higher values of root-mean-square surface roughness (R_q) of 0.2−1.5 nm, and tending to increase the surface energy. Because the low-M_w PS−$Si(CH_3)_2Cl$ chains had relatively smaller R_g values, but higher −Cl fractions relative to the high-M_w polymers, the 8 and 26 kDa PS grafted to the SiO_2 surfaces had much higher density than the 108 and 135 kDa PS. Additionally, the low-M_w *g*PS had a brush-like compact structure with a σ value $\geq$ 0.1 chains nm^{-2}, while other high-M_w *g*PS chains showed a "pancake" structure. In this case, the density of the PS chains grafted onto the surfaces significantly affected the self-assembly of solution-processed TES-ADT, as a solute. Low-density *g*PS layers were found to interfere with the crystallization of TES-ADT, causing drastic decreases in crystal grain size and π-conjugated orientation. The concentrated *g*PS layers on the SiO_2 surface could yield high electrical performance of TES-ADT OFETs with the top source/drain (S/D) electrodes showing μ_{FET} = 2.1 $cm^2\ V^{-1}\ s^{-1}$ relative to the poor electrical device (μ_{FET} = 0.8 $cm^2\ V^{-1}\ s^{-1}$) developed on coarse *g*PS layers, which disclosed the SiO_2 surface.

2. EXPERIMENTAL SECTION

2.1. Materials and Device Preparation. TES-ADT was synthesized according to the procedure described by Anthony et al.[28] Briefly, a 300 nm-thick SiO_2 layer thermally grown on a highly *n*-doped Si substrate was used as an oxide gate dielectric. The SiO_2/Si substrates were first cleaned by boiling in acetone, then treated by UV-ozone (UVO_3) exposure for 30 min. PS−$Si(CH_3)_2Cl$ chains with M_w values of 8, 26, 108, and 135 kDa were purchased from Polymer Source Inc., as end-functionalized polymers. The polymers were first dissolved in toluene to give a final volume of 0.6 vol %. The solutions were then spun-cast onto UVO_3-treated SiO_2 surfaces with popular hydroxyl (−OH) moieties inside a N_2-purged glovebox. Next, PS−$Si(CH_3)_2Cl$ films were thermally annealed at 100 °C for 1 h (Figure 1). The annealed PS−$Si(CH_3)_2Cl$ films were subsequently solvent-rinsed with excessive toluene, then thoroughly sonified in the same solvent for 3 min to remove the unreacted polymer residues. Next, 1 vol % TES-ADT solutions dissolved in 1,2-dichloroethane (DCE) were spun-cast onto the PS grafted to the SiO_2 layer (referred to as the *g*PS-SiO_2)/Si substrates. The cast TES-ADT films were further solvent-annealed in a closed jar under a vaporized DCE atmosphere for 15−20 min. Finally, top contacted S/D electrodes were fabricated via thermal evaporation of Au through a shadow mask onto the TES-ADT films.

2.2. Characterization. The surface hydrophobicity and thickness of the different M_w *g*PS-SiO_2 dielectrics were characterized by water contact angle and X-ray reflectivity (XRR) analyses, respectively. Atomic force microscopy (AFM, Multimode 8, Bruker) was also performed to investigate the surface coverage of the *g*PS layers onto the SiO_2 substrates. The crystalline structures of the solvent-assisted TES-ADT films on the *g*PS-SiO_2 dielectrics were then systematically investigated by optical microscopy (OM, Eclipse LV100N, Nikon), AFM, and synchrotron-based grazing-incidence X-ray diffraction (GIXD, beamline 9A, Pohang Acceleration Laboratory, Korea), respectively. The electrical characteristics of all of the OFETs were measured in a N_2-purged glovebox (H_2O < 0.1 ppm; O_2 < 0.1 ppm) at room temperature using a Keithley 4200 SCS. The μ_{FET} and threshold voltage (V_{th}) values were calculated in the saturation regime using the equation $I_D = \mu_{FET} C_i W (2L)^{-1} (V_G - V_{th})^2$, where C_i is the capacitance of the gate dielectrics. The C_i of the dielectrics, which were sandwiched between the Au dots and highly doped *n*-type (100) Si substrate, were measured using an Agilent 4284 precision LCR meter.

3. RESULTS AND DISCUSSION

Most inorganic oxides (e.g., SiO_2, Al_2O_3) or high-k polymer dielectrics for low-voltage OFETs have hydrophilic surface characteristics, while organic semiconductors typically have low surface energies (γ). The large differences in γ at the semiconductor−dielectric interface lead to significant degradation of the crystalline structures of both vacuum- and solution-processed organic semiconductors formed on these surfaces, resulting in reduced crystallinity, grain boundary (GB), and crystal orientation.[29−31] As mentioned above, oxide or conventional dielectric surfaces have commonly been treated with SAMs or polymers to minimize the mismatch in γ between dielectrics and organic semiconductors.[31] When organic semiconducting films are solution-cast onto polymer-treated surfaces, the surface-modified layers should maintain a consistent wettability against hydrophilic oxides via grafting of polymers to/from active moieties on the surface or polymer cross-linking.[32−34]

Here, 300 nm-thick SiO_2 layers were treated with PS−$Si(CH_3)_2Cl$ chains, after which the polymer-SiO_2 bilayers were used as gate dielectrics. Following thermal annealing of the spun-cast PS−$Si(CH_3)_2Cl$ films at 100 °C for 60 min, all PS−$Si(CH_3)_2Cl$ chains could be chemically grafted onto the UVO_3-treated SiO_2 surfaces with hydroxyl (−OH) moieties (see the Experimental Section). Figure 2 shows the M_w-dependent water contact angles (θ_{water}) of the PS−$Si(CH_3)_2Cl$ coated SiO_2 dielectrics before and after solvent-rinsing. When compared to the UVO_3-treated SiO_2 surface showing a θ_{water} value of below 40°, all of the annealed PS−$Si(CH_3)_2Cl$ coated SiO_2 dielectrics showed a θ_{water} value of 93−95°. This value was similar to the 95 ± 1° of a typical PS-coated surface, which easily became hydrophilic at below 40° after rinsing.[22] The topmost polymeric surfaces could maintain hydrophobicity even after cleaning the surfaces with excessive toluene, suggesting that the gPS chains are chemically coupled to the SiO_2 surfaces. However, the hydrophobicity of the solvent-rinsed gPS surfaces degraded slightly from 94° to 88° as the M_w of the gPS chains increased (see the red ○ in Figure 2), suggesting that the surface coverage of the gPS chains on the SiO_2 substrates differed.

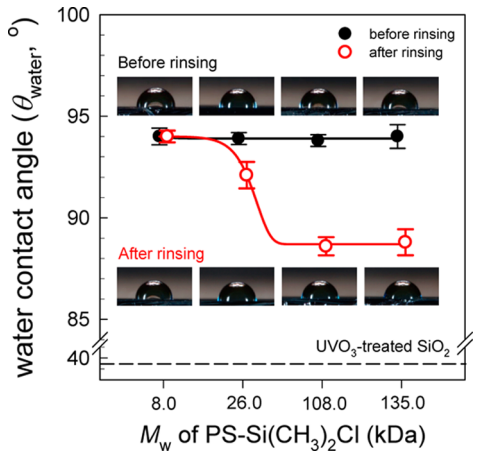

Figure 2. Variations in water contact angle (θ_{water}) of the polymer treated-SiO_2 surfaces with the different M_w PS−$Si(CH_3)_2Cl$ modifiers before (●) and after solvent-rinsing (red ○).

Figure 3 shows the AFM topographies of the different M_w gPS-SiO_2 dielectrics. The AFM topography of the 8 kDa gPS-SiO_2 dielectric showed homogeneous and smooth surface with a root-mean-square surface roughness (R_q) of 0.22 nm, comparable to 0.20 nm for a thermally grown SiO_2 surface (see Table 1). However, as the M_w of the polymers used increased, the resulting gPS-SiO_2 bilayers showed nanopinholes (for 26 kDa), bicontinuous polymer layers (for 108 kDa), and discrete polymer islands (for 135 kDa) on the SiO_2 surfaces. These surface changes resulted in drastic increases in R_q values from 0.22 to 1.47 nm. The M_w-dependent surface coverage of the gPS chains is primarily related to a decrease in both the reaction activity and the mole fraction of the −$Si(CH_3)_2Cl$ moiety of the high-M_w polymer chain near the SiO_2 surfaces due to an increase in hydrodynamic volume.

As shown in Figure 4, high-M_w polymers with a larger R_g and lower fraction of the chain-end had a much lower possibility of containing an active end moiety being positioned near the −OH-rich SiO_2 surface. During thermal annealing at 100 °C for 1 h, the coupling efficiency between the two reactive moieties decreased significantly as the M_w of the polymers near the SiO_2 surface increased. The resulting high-M_w gPS-SiO_2 surfaces tended to have a heterogeneous and irregular texture after removal of the locally unreacted polymer residue (see Figure 4b).

X-ray reflectivity (XRR) analysis was conducted to obtain information regarding the overall uniformity and thickness of these gPS layers on the SiO_2 substrates (Figure 5). The XRR profiles of the 8 and 26 kDa gPS-SiO_2 bilayers indicated periodic peak intervals (ΔQ) of 0.131 and 0.152 $Å^{-1}$,

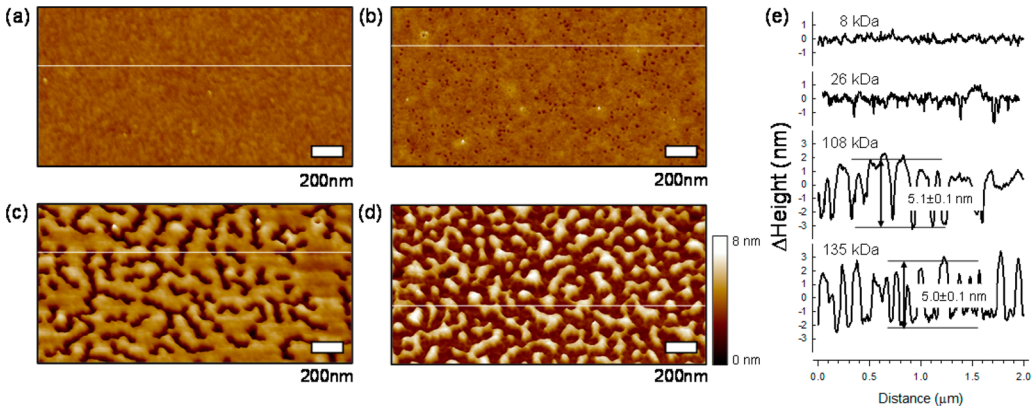

Figure 3. (a−d) AFM topographies of different M_w gPS-SiO_2 dielectric substrates: (a) 8 kDa (R_q = 0.22 nm); (b) 26 kDa (R_q = 0.37 nm); (c) 108 kDa (R_q = 1.29 nm); (d) 135 kDa (R_q = 1.47 nm). (e) Cross-sectional AFM height profiles extracted from the white lines in (a)−(d).

Table 1. Characteristics of M_w-Dependent *g*PS Layers on the SiO_2 Surfaces

*g*PS (kDa)	M_w (kg mol^{-1})	ΔQ_z (Å^{-1})	L_{PS} (nm)[a]	$\langle R_g^2\rangle^{1/2}$ (nm)[b]	σ (chains nm^{-2})	grafting type	capacitance (C_i, nF cm^{-2})
8	8.0	0.131	4.81	1.79	0.38	brush	10.4
26	26.2	0.152	4.16	3.24	0.11	brush	10.6
108	107.5		5.10	6.63	3.0×10^{-2}	pancake	10.6
135	135.0		5.00	7.35	2.3×10^{-2}	pancake	10.7

[a]Calculated by XRR or AFM. [b]Calculated by the following equation:[38] $\langle R_g^2\rangle^{1/2} = (C_\infty M_w l^2/6M_o)^{1/2}$, where $\langle R_g^2\rangle^{1/2}$ is the radius of gyration, C_∞ (=10) is the characteristic ratio of PS, l (=0.153 nm) is the length between carbon−carbon single bond, and M_o (=104 g mol^{-1}) is the molecular weight of the styrene unit.

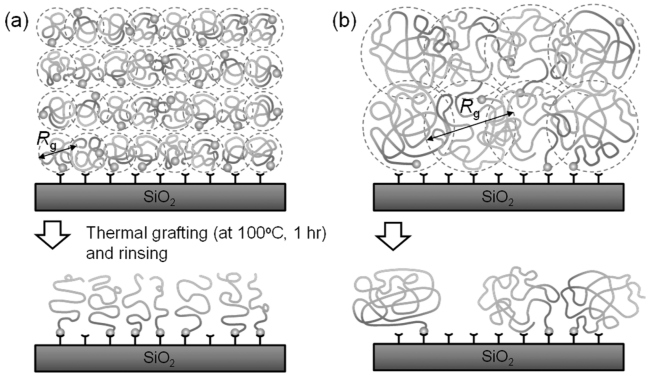

Figure 4. Schemes of different grafting densities of (a) low- and (b) high-M_w PS−$Si(CH_3)_2Cl$ on the hydroxyl-rich SiO_2 surfaces originating from large variations in hydrodynamic volume and mole fraction of the reactive moiety of the polymers near the surface.

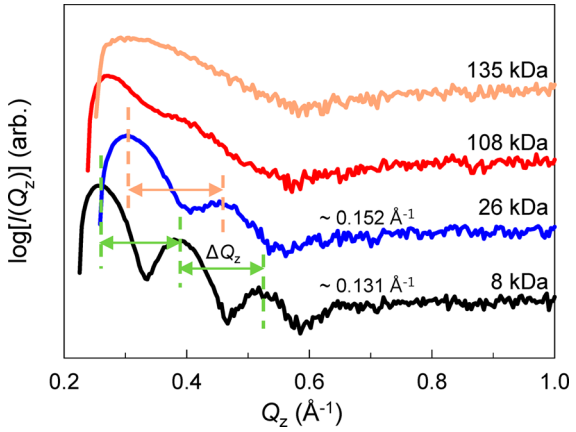

Figure 5. X-ray reflectivity (XRR) profiles of different M_w *g*PS layers on the SiO_2 dielectrics.

respectively, corresponding to PS layer thicknesses ($L_{PS} = 2\pi/\Delta Q$) of 4.81 and 4.16 nm.[35] However, the XRR of the bicontinuous or polymeric island structures on the SiO_2 substrates was scattered, without any clear sequence. Herein, L_{PS} values for the 108 and 135 kDa *g*PS layers were obtained from the cross-sectional AFM height profiles (see Figure 3e). Because of the ultrathin PS layers, all of the *g*PS-SiO_2 bilayer dielectrics had a C_i of approximately 10.4−10.7 nF cm^{-2}, comparable to 10.9 nF cm^{-2} of the untreated SiO_2 dielectric (see Table 1).

To investigate the conformation of different M_w *g*PS chains on the SiO_2 surfaces, σ values were calculated using the following equation:

$$\sigma = \rho N_A L_{PS}/M_w$$

where ρ is the density of PS (=1.05 g cm^{-3}), N_A is Avogadro's number, and M_w is the weight-average molecular weight of the *g*PS chain.

All σ values are summarized in Table 1. It is well-known that typical polymer chains do not overlap at the substrate surface at less than σ = 0.01 chains nm^{-2}. Furthermore, they tend to form a random-coil conformation in solutions of a good solvent, and polymer pancakes with a vertical collapse in a dried state.[36] In contrast, at greater than σ = 0.10 chains nm^{-2}, the chains overlapped and stretched away from the substrate surface in a good solvent, forming polymer brushes. As shown in Table 1, the σ values decreased as M_w increased in the end-functionalized PS chains used. Specifically, the σ values of the 8 and 26 kDa *g*PS chains were calculated to be 0.38 and 0.11 chains nm^{-2}, respectively, suggesting that the low-M_w (<entanglement molecular weight of PS,[37] $M_{e,PS}$ = 32 kDa) *g*PS chains may form brush-like conformations in a good solvent such as DCE. Upon initial solution casting, the polymer brushes were swollen and stretched away from the surface. However, it was estimated that the high-M_w *g*PS (>M_e, PS) chains on the SiO_2 surfaces yielded σ values of 0.03 and 0.023 chains nm^{-2}, respectively. As a solute, TES-ADT might easily diffuse into the high-M_w *g*PS layers due to the poor size exclusion driven by these low grafting densities (see Figure 6).

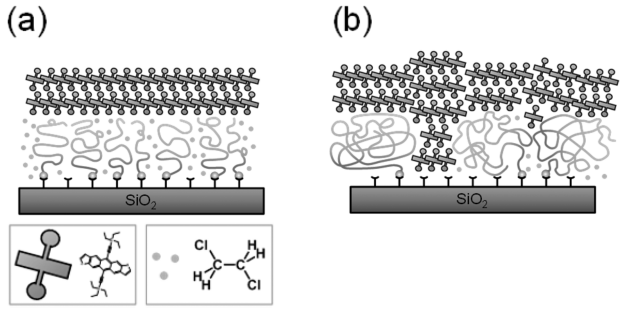

Figure 6. Conformation effects of the *g*PS chains on the self-assembly of TES-ADT solute during solution-casting: (a) on concentrated polymer brush; (b) on porous polymeric pancake layers.

The above findings were confirmed by morphological analysis of ultrathin TES-ADT films drop-cast onto the *g*PS-SiO_2 dielectrics from 0.02 vol % DCE solutions (0.2 mg mL^{-1}). Figure 7 shows the AFM topographies of the TES-ADT films cast on the *g*PS layers with different chain lengths and grafting densities. As the σ values of the *g*PS chains on the SiO_2 surfaces decreased, the self-assembled structures of TES-ADT on these layers tended to become amorphous. When compared to the layered crystal morphology of TES-ADT on the 8 kDa PS brushes, the low-concentrated *g*PS layers severely interfered with the self-assembly of π-conjugated TES-ADT onto their surfaces.

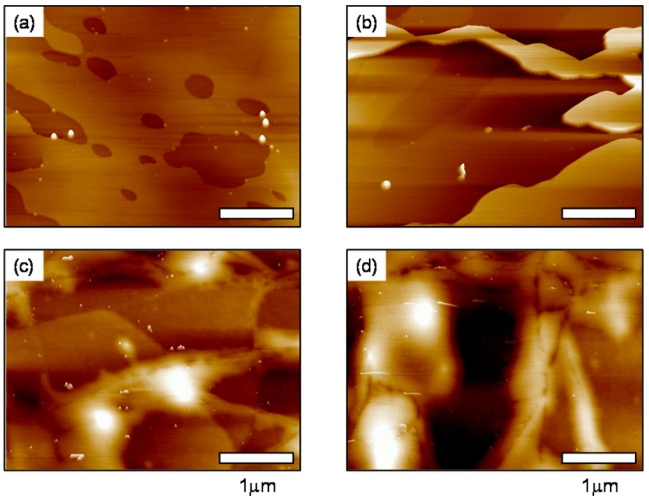

Figure 7. AFM topographies of ultrathin TES-ADT films drop-cast on the *g*PS-SiO_2 dielectrics: (a) 8 kDa; (b) 26 kDa; (c) 108 kDa; and (d) 135 kDa, respectively.

TES-ADT thin films were spun-cast on the *g*PS-SiO_2 bilayer dielectrics and subsequently solvent-annealed under a DCE-vaporized atmosphere.[39] Figure 8 shows polarized optical

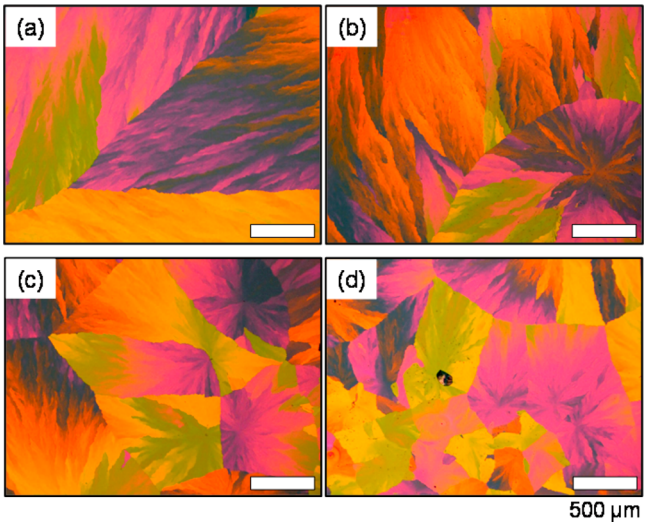

Figure 8. Polarized optical microscopy (POM) images of DCE-annealed TES-ADT films on the different M_w *g*PS-SiO_2 dielectrics: (a) 8 kDa; (b) 26 kDa; (c) 108 kDa; and (d) 135 kDa, respectively.

microscopy (POM) images of the resulting TES-ADT films based on the different M_w *g*PS-SiO_2 dielectrics. The POM images reveal discernible spherulitic crystal morphologies of the TES-ADT. The 8 kDa *g*PS layer indicated as a polymer brush could grow millimeter-sized TES-ADT crystal grains. However, the grain sizes decreased drastically as the M_w of the *g*PS chains increased. Specifically, the size of the grains on the 26 kDa *g*PS layer as a less-concentrated polymer brush decreased slightly relative to those on the 8 kDa *g*PS brush, while the 135 kDa *g*PS layer with a pancake-like texture interfered with the crystal development of TES-ADT, resulting in grain sizes of 300−800 μm. Additional AFM topographies for the topmost TES-ADT crystallites showed multilayered crystal morphologies with a step height of approximately 16 Å, while the layer stacking of percolated crystal grains was degraded and mismatched as the M_w of the *g*PS chains increased (see Figure S1 in the Supporting Information).

Synchrotron-based GIXD analysis was also performed to evaluate these TES-ADT films. Figure 9 shows the 2D GIXD

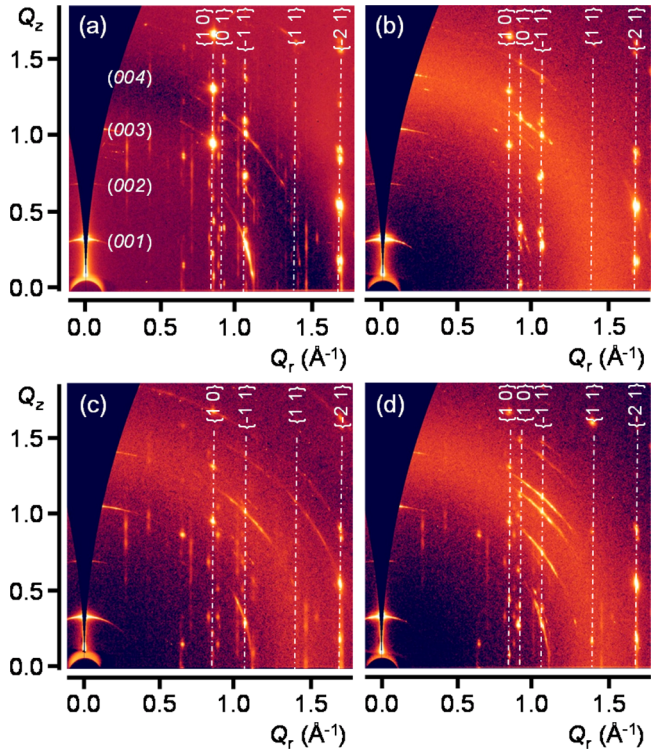

Figure 9. Two-dimensional (2D) grazing-incidence X-ray diffraction (GIXD) patterns of the DCE-annealed TES-ADT films on different M_w *g*PS-SiO_2 dielectrics: (a) 8 kDa; (b) 26 kDa; (c) 108 kDa; and (d) 135 kDa, respectively.

patterns for the DCE-annealed TES-ADT film on the *g*PS-SiO_2 dielectric series. All 2D GIXD patterns showed intense out-of-plane and in-plane reflections along the Q_z and Q_r axes, respectively. The (00*l*) reflections along the Q_z axis were related to a multilayered crystal structure of TES-ADT with a layer spacing of ∼16.7 Å. Additionally, the in-plane reflections (referred to as {*h k*}) at a given Q_r strongly supported that TES-ADT molecules were aligned with an edge-on conformation and stacked with a face-to-face overlap of π-conjugated planes in which the *ab* plane parallel to the modified SiO_2 substrate yielded π−π overlap along the lateral crystal planes. The 2D GIXD revealed that the solvent-induced TES-ADT crystals had a triclinic structure with the following unit-cell: a = 14.78 Å, b = 6.91 Å, c = 16.68 Å, α = 92.1°, β = 96.4°, γ = 105.9°.[22] As shown in Figure 9, the crystal orientations of TES-ADT on the dielectric series were affected by the R_q and σ of the *g*PS layers. On the 8 and 26 kDa *g*PS-SiO_2 dielectrics containing smooth and compact polymer brushes ($\sigma \geq 0.1$ chains nm^{-2}), the TES-ADT crystallites were preferentially oriented along the surfaces, while on the 108 and 135 kDa *g*PS systems with rough and course polymer layers ($\sigma \approx 0.03$ chains nm^{-2}) they were less-oriented, as indicated by the Debye rings scattering at Q (see Figure 9c and d). The variations in grain size, boundary, and orientation of TES-ADT on the *g*PS-SiO_2 dielectric series had a considerable effect on the long-range order of the π-conjugation path, which was expected to result in different electrical properties in OFETs.

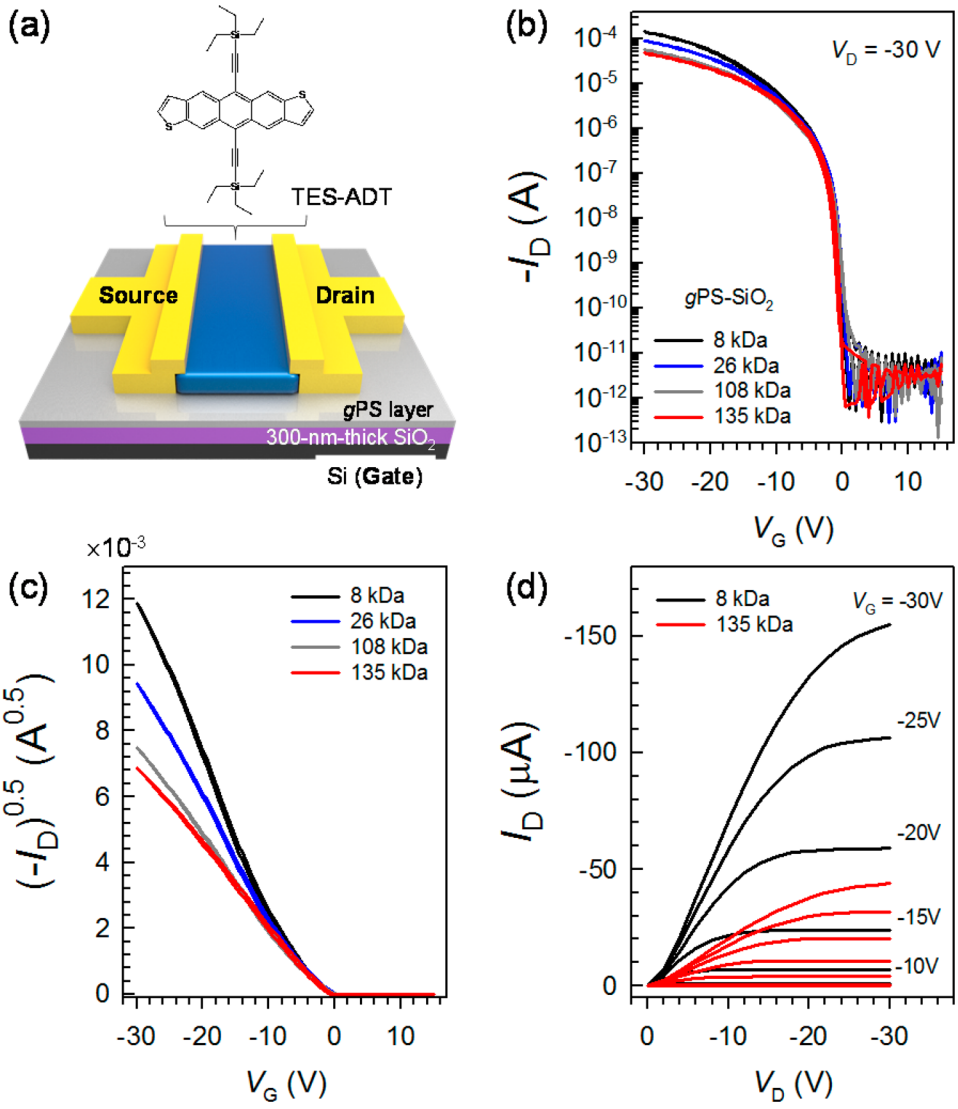

Figure 10. (a) Scheme and (b–d) electrical performances of TES-ADT OFETs: (b,c) transfer curves and (d) output curves depending on the modified-SiO_2 containing different M_w *g*PS layers. The channel length, *L*, and width, *W*, were 100 and 1500 μm, respectively.

Table 2. Electrical Characteristics of TES-ADT OFETs Based on the Different *g*PS-SiO_2 Dielectrics

OFET	dielectric	μ_{FET} (cm^2 V^{-1} s^{-1})	V_{th} (V)	SS (V $decade^{-1}$)	I_{on}/I_{off}
8 kDa sample	8 kDa *g*PS-SiO_2	2.12 ± 0.30	−2.0	0.41	1.35×10^7
26 kDa sample	26.5 kDa *g*PS-SiO_2	1.97 ± 0.15	−2.1	0.51	1.44×10^7
108 kDa sample	107.5 kDa *g*PS-SiO_2	1.15 ± 0.20	−2.5	0.54	9.14×10^6
135 kDa sample	135 kDa *g*PS-SiO_2	0.85 ± 0.10	−2.5	0.55	7.27×10^6

Top-contacted electrode OFETs were fabricated via thermal evaporation of Au through a shadow mask (L = 100 μm; W = 1500 μm) onto these TES-ADT films (see Figure 10a). Figure 10b shows the drain current–gate voltage (I_D–V_G) transfer and corresponding $(-I_D)^{0.5}$–V_G curves of the TES-ADT OFETs based on the *g*PS-SiO_2 dielectric series operated under a saturation regime (drain voltage, V_D = −30 V). The electrical characteristics of the OFETs are also summarized in Table 2. The TES-ADT OFETs showed typical *p*-type transistor characteristics (see Figure 10d), and all of the I_D–V_G transfer curves of the *g*PS-assisted SiO_2 systems showed negligible hysteresis during the V_G sweep when compared to the untreated SiO_2-based device showing V_G-sweep hysteresis and a relatively positive turn-on voltage of approximately 5 V (see Figure S2 in the Supporting Information). This is attributed to the hydrophobic *g*PS layer, which could deactivate or cover the charge-trap sites on the polar gate dielectric. However, the transfer curves of TES-ADT OFETs on the *g*PS-SiO_2 dielectric series indicate discernible device performance. The 8 kDa *g*PS-SiO_2 system containing the concentrated polymer brush showed the highest electrical performance (μ_{FET} = 2.1 ± 0.3 cm^2 V^{-1} s^{-1}, V_{th} = −2.0 V, SS = 0.41 V $decade^{-1}$, and $I_{on}/I_{off} > 10^7$). In contrast, the less-crystalline TES-ADT films on the 135 kDa *g*PS-SiO_2 dielectric showed relatively poor electrical properties in OFET (μ_{FET} = 0.8 ± 0.1 cm^2 V^{-1} s^{-1}, V_{th} = −2.5 V, SS = 0.55 V $decade^{-1}$, and $I_{on}/I_{off} \approx 7 \times 10^6$).

The introduction of ultrathin polymer interlayers between solution-processed semiconductors via a simple grafting

method of solution-processable end-functionalized polymers to oxide surfaces led to dielectric coatings, which effectively deactivated the surface polar moieties related to the interfacial charge traps in OFETs. As a result, the hydrophobic polymer-grafted SiO_2 bilayer dielectrics could fabricate high performance OFETs. Unlike typical SAMs with short chain lengths, it is important to optimize the density of end-functionalized polymers grafted to oxide surfaces for high-performance solution-processed OFET fabrication.

4. CONCLUSION

Polystyrene (PS)-grafted to SiO_2 (referred to as *g*PS-SiO_2) bilayers were used as organic-oxide hybrid gate dielectrics to fabricate solution-processed triethylsilylethynyl anthradithiophene (TES-ADT) organic field-effect transistors (OFETs). The dielectric surface properties were significantly altered by the areal grafting densities of different molecular weight (M_w) PS chains attached with the dimethylchlorosilane end to the SiO_2 surfaces. The surface properties of the *g*PS-SiO_2 dielectrics were affected by the chain lengths of the polymers, with higher M_w PS−$Si(CH_3)_2Cl$ yielding higher values of root-mean-square surface roughness (R_q) from 0.2 to 1.5 nm and increased surface energy. These findings were mainly related to changes in the hydrodynamic volume and the reactive chloro (−Cl) fraction of the polymer. Because the low-M_w PS−$Si(CH_3)_2Cl$ chains had relatively smaller R_g but higher −Cl fractions relative to the high-M_w polymers, the low-M_w PS grafted to the SiO_2 surfaces had much higher density than the 108 and 135 kDa samples. Specifically, the 8 and 26 kDa *g*PS had a brush-like compact structure with a σ value of greater than 0.1 chains nm^{-2}, but other high-M_w *g*PS chains were estimated to have a "pancake" structure. The self-assembly of solution-processable TES-ADT as a solute onto the surface was significantly influenced by the different areal graft densities of PS chains. The low-density *g*PS layers were found to interfere with the crystallization of TES-ADT, causing drastic decreases in crystal grain size and π-conjugated orientation. The concentrated *g*PS layers on the SiO_2 surface led to higher electrical performance of TES-ADT OFETs, with top contacted S/D electrodes (channel length = 100 μm and channel width = 1500 μm) showing a higher μ_{FET} = 2.1 $cm^2\ V^{-1}\ s^{-1}$ relative to a poor electrical device (μ_{FET} = 0.8 $cm^2\ V^{-1}\ s^{-1}$) developed on the less dense *g*PS-SiO_2 surface.

■ ASSOCIATED CONTENT

Supporting Information

AFM of DCE-annealed TES-ADT films; transfer curve of TES-ADT OFET based on untreated SiO_2 dielectric. This material is available free of charge via the Internet at http://pubs.acs.org.

■ AUTHOR INFORMATION

Corresponding Author

*Phone: +82-32-860-7494. E-mail: hcyang@inha.ac.kr.

Notes

The authors declare no competing financial interest.

■ ACKNOWLEDGMENTS

This work was supported by grants from the Center for Advanced Soft Electronics under the Global Frontier Research Program (2012M3A6A5055225), General Research Program (2013R1A12063963) of the Ministry of Education, Science, and Technology (MEST), Korea. This work was also supported by the International collaborative R&D program (N0000678, Joint development of highly flexible materials & processes for more than 10,000 times bendable TFT array, with application to flexible display) funded by the Ministry of Trade, Industry and Energy (MOTIE, Korea).

■ ABBREVIATIONS

PS = polystyrene
TES-ADT = triethylsilylethynyl anthradithiophene
OFET = organic field-effect transistor
M_w = weight-average molecular weight
SiO_2 = silicon dioxide
*g*PS = grafted polystyrene
*g*POLY = grafted polymer
AFM = atomic force microscopy
GIXD = grazing-incidence X-ray diffraction
OM = optical microscopy

■ REFERENCES

(1) Jurchescu, O. D.; Popinciuc, M.; van Wees, B. J.; Palstra, T. T. M. Interface-Controlled, High-Mobility Organic Transistors. *Adv. Mater.* **2007**, *19*, 688−692.
(2) Ebata, H.; Izawa, T.; Miyazaki, E.; Takimiya, K.; Ikeda, M.; Kuwabara, H.; Yui, T. Highly Soluble [1]Benzothieno[3,2-*b*]-benzothiophene (BTBT) Derivatives for High-Performance, Solution-Processed Organic Field-Effect Transistors. *J. Am. Chem. Soc.* **2007**, *129*, 15732−15733.
(3) Sirringhaus, H. 25th Anniversary Article: Organic Field-Effect Transistors: The Path Beyond Amorphous Silicon. *Adv. Mater.* **2014**, *26*, 1319−1335.
(4) Zen, A.; Pflaum, J.; Hirschmann, S.; Zhuang, W.; Jaiser, F.; Asawapirom, U.; Rabe, J. P.; Scherf, U.; Neher, D. Effect of Molecular Weight and Annealing of Poly(3-hexylthiophene)s on the Performance of Organic Field-Effect Transistors. *Adv. Funct. Mater.* **2004**, *14*, 757−764.
(5) Kang, I.; Yun, H.-J.; Chung, D. S.; Kwon, S.-K.; Kim, Y.-H. Record High Hole Mobility in Polymer Semiconductors via Side-Chain Engineering. *J. Am. Chem. Soc.* **2013**, *135*, 14896−14899.
(6) Sirringhaus, H.; Tessler, N.; Friend, R. H. Integrated Optoelectronic Devices Based on Conjugated Polymers. *Science* **1998**, *280*, 1741−1744.
(7) Di, C.-A.; Liu, Y.; Yu, G.; Zhu, D. Interface Engineering: An Effective Approach toward High-Performance Organic Field-Effect Transistors. *Acc. Chem. Res.* **2009**, *42*, 1573−1583.
(8) Yoon, M.-H.; Kim, C.; Facchetti, A.; Marks, T. J. Gate Dielectric Chemical Structure−Organic Field-Effect Transistor Performance Correlations for Electron, Hole, and Ambipolar Organic Semiconductors. *J. Am. Chem. Soc.* **2006**, *128*, 12851−12869.
(9) Yoon, M.-H.; Yan, H.; Facchetti, A.; Marks, T. J. Low-Voltage Organic Field-Effect Transistors and Inverters Enabled by Ultrathin Cross-Linked Polymers as Gate Dielectrics. *J. Am. Chem. Soc.* **2005**, *127*, 10388−10395.
(10) Dong, H.; Fu, X.; Liu, J.; Wang, Z.; Hu, W. 25th Anniversary Article: Key Points for High-Mobility Organic Field-Effect Transistors. *Adv. Mater.* **2013**, *25*, 6158−6183.
(11) Miozzo, L.; Yassar, A.; Horowitz, G. Surface Engineering for High Performance Organic Electronic Devices: The Chemical Approach. *J. Mater. Chem.* **2010**, *20*, 2513−2538.
(12) Boudinet, D.; Benwadih, M.; Altazin, S.; Verilhac, J.-M.; De Vito, E.; Serbutoviez, C.; Horowitz, G.; Facchetti, A. Influence of Substrate Surface Chemistry on the Performance of Top-Gate Organic Thin-Film Transistors. *J. Am. Chem. Soc.* **2011**, *133*, 9968−9971.
(13) Klauk, H.; Zschieschang, U.; Pflaum, J.; Halik, M. Ultralow-Power Organic Complementary Circuits. *Nature* **2007**, *445*, 745−748.
(14) Kagan, C. R.; Afzali, A.; Martel, R.; Gignac, L. M.; Solomon, P. M.; Schrott, A. G.; Ek, B. Evaluations and Considerations for Self-

Assembled Monolayer Field-Effect Transistors. *Nano Lett.* **2002**, *3*, 119−124.
(15) Kobayashi, S.; Nishikawa, T.; Takenobu, T.; Mori, S.; Shimoda, T.; Mitani, T.; Shimotani, H.; Yoshimoto, N.; Ogawa, S.; Iwasa, Y. Control of Carrier Density by Self-Assembled Monolayers in Organic Field-Effect Transistors. *Nat. Mater.* **2004**, *3*, 317−322.
(16) Rodriguez, A. B.; Tomlinson, M. R.; Khodabakhsh, S.; Chang, J.-F.; Cousin, F.; Lott, D.; Sirringhaus, H.; Huck, W. T. S.; Higgins, A. M.; Geoghegan, M. All-Polymer Field-Effect Transistors Using a Brush Gate Dielectric. *J. Mater. Chem. C* **2013**, *1*, 7736−7741.
(17) Ma, H.; Yip, H.-L.; Huang, F.; Jen, A. K. Y. Interface Engineering for Organic Electronics. *Adv. Funct. Mater.* **2010**, *20*, 1371−1388.
(18) Pinto, J. C.; Whiting, G. L.; Khodabakhsh, S.; Torre, L.; Rodríguez, A.; Dalgliesh, R. M.; Higgins, A. M.; Andreasen, J. W.; Nielsen, M. M.; Geoghegan, M.; Huck, W. T. S.; Sirringhaus, H. Organic Thin Film Transistors with Polymer Brush Gate Dielectrics Synthesized by Atom Transfer Radical Polymerization. *Adv. Funct. Mater.* **2008**, *18*, 36−43.
(19) Li, L.; Hu, W.; Chi, L.; Fuchs, H. Polymer Brush and Inorganic Oxide Hybrid Nanodielectrics for High Performance Organic Transistors. *J. Phys. Chem. B* **2010**, *114*, 5315−5319.
(20) Whiting, G. L.; Snaith, H. J.; Khodabakhsh, S.; Andreasen, J. W.; Breiby, D. W.; Nielsen, M. M.; Greenham, N. C.; Friend, R. H.; Huck, W. T. S. Enhancement of Charge-Transport Characteristics in Polymeric Films Using Polymer Brushes. *Nano Lett.* **2006**, *6*, 573−578.
(21) Li, L.; Zhang, Y.; Li, H.; Tang, Q.; Jiang, L.; Chi, L.; Fuchs, H.; Hu, W. Battery Drivable Organic Single-Crystalline Transistors Based on Surface Grafting Ultrathin Polymer Dielectric. *Adv. Funct. Mater.* **2009**, *19*, 2987−2991.
(22) Kim, S. H.; Jang, M.; Yang, H.; Anthony, J. E.; Park, C. E. Physicochemically Stable Polymer-Coupled Oxide Dielectrics for Multipurpose Organic Electronic Applications. *Adv. Funct. Mater.* **2011**, *21*, 2198−2207.
(23) Zhao, B.; Brittain, W. J. Polymer Brushes: Surface-Immobilized Macromolecules. *Prog. Polym. Sci.* **2000**, *25*, 677−710.
(24) de Gennes, P. G. Conformations of Polymers Attached to an Interface. *Macromolecules* **1980**, *13*, 1069−1075.
(25) de Gennes, P. G. Polymers at an Interface; a Simplified View. *Adv. Colloid Interface Sci.* **1987**, *27*, 189−209.
(26) Currie, E. P. K.; Norde, W.; Cohen Stuart, M. A. Tethered Polymer Chains: Surface Chemistry and Their Impact on Colloidal and Surface Properties. *Adv. Colloid Interface Sci.* **2003**, *100−102*, 205−265.
(27) Szleifer, I.; Carignano, M. A. Tethered Polymer Layers: Phase Transitions and Reduction of Protein Adsorption. *Macromol. Rapid Commun.* **2000**, *21*, 423−448.
(28) Payne, M. M.; Odom, S. A.; Parkin, S. R.; Anthony, J. E. Stable, Crystalline Acenedithiophenes with up to Seven Linearly Fused Rings. *Org. Lett.* **2004**, *6*, 3325−3328.
(29) Yang, S. Y.; Shin, K.; Park, C. E. The Effect of Gate-Dielectric Surface Energy on Pentacene Morphology and Organic Field-Effect Transistor Characteristics. *Adv. Funct. Mater.* **2005**, *15*, 1806−1814.
(30) Jang, Y.; Cho, J. H.; Kim, D. H.; Park, Y. D.; Hwang, M.; Cho, K. Effects of the Permanent Dipoles of Self-Assembled Monolayer-Treated Insulator Surfaces on the Field-Effect Mobility of a Pentacene Thin-Film Transistor. *Appl. Phys. Lett.* **2007**, *90*, 132104.
(31) Yang, H.; Kim, S. H.; Yang, L.; Yang, S. Y.; Park, C. E. Pentacene Nanostructures on Surface-Hydrophobicity-Controlled Polymer/SiO_2 Bilayer Gate-Dielectrics. *Adv. Mater.* **2007**, *19*, 2868−2872.
(32) Park, K.; Park, S. H.; Kim, E.; Kim, J.-D.; An, S.-Y.; Lim, H. S.; Lee, H. H.; Kim, D. H.; Ryu, D. Y.; Lee, D. R.; Cho, J. H. Polymer Brush As a Facile Dielectric Surface Treatment for High-Performance, Stable, Soluble Acene-Based Transistors. *Chem. Mater.* **2010**, *22*, 5377−5382.
(33) Wang, C.; Lee, W.-Y.; Nakajima, R.; Mei, J.; Kim, D. H.; Bao, Z. Thiol−ene Cross-Linked Polymer Gate Dielectrics for Low-Voltage Organic Thin-Film Transistors. *Chem. Mater.* **2013**, *25*, 4806−4812.
(34) Kronemeijer, A. J.; Pecunia, V.; Venkateshvaran, D.; Nikolka, M.; Sadhanala, A.; Moriarty, J.; Szumilo, M.; Sirringhaus, H. Two-Dimensional Carrier Distribution in Top-Gate Polymer Field-Effect Transistors: Correlation between Width of Density of Localized States and Urbach Energy. *Adv. Mater.* **2014**, *26*, 728−733.
(35) Chechetkina, E. A. The First Sharp Diffraction Peak in Glasses and in Other Amorphous Substances. *J. Phys.: Condens. Matter* **1993**, *5*, L527−L530.
(36) Minko, S. Responsive Polymer Brushes. *J. Macromol. Sci., Polym. Rev.* **2006**, *46*, 397−420.
(37) Wool, R. P. Polymer Entanglements. *Macromolecules* **1993**, *26*, 1564−1569.
(38) Singh, L.; Ludovice, P. J.; Henderson, C. L. Influence of Molecular Weight and Film Thickness on the Glass Transition Temperature and Coefficient of Thermal Expansion of Supported Ultrathin Polymer Films. *Thin Solid Films* **2004**, *449*, 231−241.
(39) Dickey, K. C.; Anthony, J. E.; Loo, Y. L. Improving Organic Thin-Film Transistor Performance through Solvent-Vapor Annealing of Solution-Processable Triethylsilylethynyl Anthradithiophene. *Adv. Mater.* **2006**, *18*, 1721−1726.